Mode selection for electrostatic beam resonators based on motional resistance and quality factor

Jeong Hoon Ryou[1,2] and Jason J. Gorman[1,a)]
[1]National Institute of Standards and Technology, 100 Bureau Drive, Stop 8212, Gaithersburg, Maryland 20899-8212, USA
[2]Department of Mechanical Engineering, University of Michigan, G.G. Brown Laboratory, 2350 Hayward, Ann Arbor, Michigan 48109, USA

(Received 12 April 2016; accepted 17 November 2016; published online 6 December 2016)

An analytical comparison between the fundamental mode and higher modes of vibration for an electrostatic beam resonator is presented. Multiple mode numbers can be matched to a desired resonance frequency through appropriate scaling. Therefore, it is important to determine which mode yields the best performance. A dynamic model of the resonator is derived and then used to determine the motional resistance for each mode. The resulting equation provides the basis for comparing performance between modes using motional resistance and quality factor. As a demonstration of the approach, a quality factor model that has been previously validated experimentally is introduced. Numerical results for silicon resonators indicate that the fundamental mode can provide a lower motional resistance and higher quality factor when the resonators under comparison have the same aspect ratio or the same stiffness. [http://dx.doi.org/10.1063/1.4971249]

I. INTRODUCTION

Microelectromechanical (MEMS) resonators have received considerable attention over the last decade for applications in wireless communications,[1] timing and frequency control,[2,3] and biochemical sensing,[4] among others. In many of these applications, there is strong interest in increasing the resonance frequencies that can be attained in order to extend capabilities (e.g., resonators operating in the GHz range will result in more efficient sharing of the wireless communications spectrum) or to improve sensitivity (e.g., chemical mass sensing resolution improves with increasing frequency). Different modes of vibration, such as flexural, contour, thickness, and shear modes, achieve different frequency ranges. Additionally, resonance frequencies are proportional to the acoustic velocity of the materials used. As a result, the mode of vibration and materials used must be selected carefully to match with the frequency requirements for a given application. For a resonator design operating with a specific mode of vibration and optimized materials, there are two ways to further increase its operating frequency: (1) scale down its dimensions since resonance frequencies are proportional to $1/S$, where S is the scaling factor, or (2) use a higher vibrational mode number rather than operating at the fundamental resonance frequency. Both of these approaches often result in weaker transduction and reduced quality factors. Therefore, selection between the two approaches is not obvious and detailed modeling is required to determine which approach yields the optimal MEMS resonator design.

This paper investigates the above problem for one class of MEMS resonators: the electrostatic beam resonator. This was one of the first types of MEMS resonators to be developed[5] and has been studied widely at the microscale[6–8] and nanoscale.[9,10] The electrostatic beam resonator is composed of a constrained beam (e.g., clamped-clamped, clamped-free, free-free), an electrode for applying an electrostatic force to excite vibrations in the beam, and an electrode for capacitive measurement of the displacement of the vibrating beam. In order to achieve a desired resonance frequency, the beam dimensions can be scaled so that either the fundamental resonance frequency or a higher mode number matches the desired frequency, where the former resonator is smaller than the latter. Examples of both approaches include nanoelectromechanical resonators[9,10] and higher mode free-free beam resonators,[11] respectively. The primary question explored in this paper is how does one determine which of these two approaches yields the resonator with the best performance. Two of the most important performance metrics for resonators are used to answer this question: motional resistance and quality factor. The motional resistance is a measure of the amplitude of the output current for a given input voltage, while the quality factor determines the resonator's frequency selectivity. It is shown that by applying these metrics, one can select the best approach based on the frequency range of interest and the dimensional constraints due to fabrication.

In Section II, an analytical model of the dynamics of a prototypical electrostatic beam resonator is derived. This model is then used to derive the motional impedance, and subsequently the motional resistance, for any flexural mode and electrode length relative to the beam length. A framework for comparing modes using ratios of motional resistance and quality factor between modes is then presented. In particular, the motional resistance ratio is discussed with respect to different scaling laws between the fundamental and higher modes. In order to demonstrate the proposed comparison method, a model for quality factor in beam resonators that has been previously experimentally validated is then introduced for the same scaling conditions. Numerical results for silicon electrostatic resonators are presented to demonstrate how geometric scaling can affect mode selection between the fundamental and higher modes.

a)E-mail: gorman@nist.gov

II. RESONATOR DYNAMIC MODEL

The electrostatic beam resonator considered here, as shown in Fig. 1, is similar to those investigated in Refs. 6 and 8–10. The resonator has a single clamped-clamped flexural beam and a pair of electrodes, one to excite vibrations using electrostatic force and the other to measure the beam vibrations through capacitive sensing. As shown in Fig. 1(b), a radio frequency (RF) input voltage, V_{AC}, excites the resonator and an output current, i_o, results due to the motion of the beam and the DC bias voltage, V_b, applied to the beam. In this section, a dynamic model that describes the relationship between V_{AC} and i_o is derived. This model is then linearized, and the voltage-current relationship is presented for a single mode of the resonator, thereby providing an equation for determining the motional resistance.

Several dynamic models have been presented for the resonator shown in Fig. 1.[8,9,12] The total dynamic response of the resonator is described by the equations of motion for the vibrating beam and an equation relating beam vibrations to the output current. First, the Euler-Bernoulli beam equation with electrostatic forces is defined as[9]

$$\rho bh\frac{\partial^2 w}{\partial t^2}+EI\frac{\partial^4 w}{\partial x^4}=\frac{\varepsilon_0 hc_f f_e(x)V^2}{2(g-w)^2}-\frac{\varepsilon_0 hc_f f_e(x)V_b^2}{2(g+w)^2}, \quad (1)$$

where ρ is the material density, E is the Young's modulus, I is the area moment of inertia, w is the deflection of the beam as a function of the position, x, on the beam, b is the beam width, and h is the beam thickness. The right side of Eq. (1) describes the electrostatic forces, where g is the nominal gap between the beam and electrodes, V is the summation of the bias voltage, V_b, and the RF voltage, V_{AC}, ε_0 is the vacuum permittivity, and c_f is a fringing field correction factor.[9] The length of the electrodes, L_e, is introduced through $f_e(x)$, which is defined as

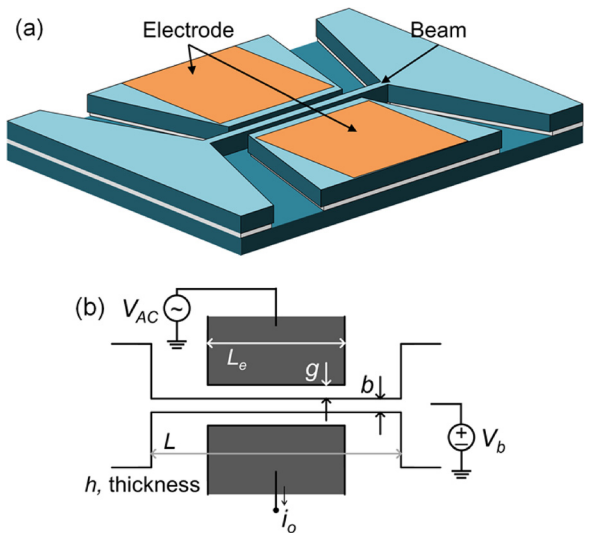

FIG. 1. Schematics of the electrostatic beam resonator: (a) solid model and (b) electromechanical diagram, where L, b, and h are the length, width, and thickness of the beam, L_e is the electrode length, g is the nominal gap between the beam and electrodes, V_{AC} is the RF input voltage, V_b is the bias voltage, and i_o is the output current.

$$f_e(x)=\begin{cases}0 & for \quad x<\dfrac{L-L_e}{2}\\ 1 & for \quad \dfrac{L-L_e}{2}\le x\le\dfrac{L+L_e}{2}\\ 0 & for \quad x>\dfrac{L+L_e}{2}.\end{cases} \quad (2)$$

Unlike previous models,[8,9,12] axial force due to residual stress and the nonlinearity due to mid-plane stretching are not included here. Residual stress will have minimal effect on mode selection because for a given material, it shifts the resonance frequency and quality factor for all mode numbers in the same direction. Additionally, the residual stress is low in most single crystal resonators, which are most commonly used. Regarding the omission of the nonlinear terms, the motional impedance is ill defined for nonlinear resonators, so the focus here is on the small amplitude linear response.

The charge measured at the output electrode, q_o, can be expressed as

$$q_0=V_b\int_0^L C\,dx=V_b\int_0^L\frac{\varepsilon_0 c_f h f_e(x)}{g+w}\,dx, \quad (3)$$

where C is the capacitance per unit length. Noting that $i_0=\dot{q}_0$, the output current is expressed as

$$i_0=-\varepsilon_0 hc_f V_b\int_0^L\frac{f_e(x)}{(g+w)^2}\dot{w}\,dx. \quad (4)$$

Equations (1) and (4) describe the nonlinear relationship between the input voltage, V, and the output current, i_o. In order to derive the motional impedance, we must linearize these dynamic equations.

Equations (1) and (4) can be linearized about the equilibrium position, w_0, for a given value of V_b. Looking at Eq. (1), it can be shown that when an arbitrary bias voltage, V_b, is applied to the resonator and $V_{AC}=0$, there is no displacement due to balanced electrostatic forces from the two electrodes. Therefore, the equilibrium position is $w_0=0$. Equation (3) can then be linearized about this equilibrium point using a Taylor series expansion to first order, where the linearized system can be written as

$$\rho bh\frac{\partial^2 w}{\partial t^2}+EI\frac{\partial^4 w}{\partial x^4}=\frac{2\varepsilon_0 hc_f f_e(x)V_b^2}{g^3}w-\frac{\varepsilon_0 hc_f f_e(x)V_b}{g^2}V_{AC}. \quad (5)$$

The first term on the right-hand side of Eq. (5) represents the linearized electrostatic stiffness, which can be disregarded within the context of this analysis since its influence on the resonance frequencies, and therefore the motional impedance, is negligible. Hence, Eq. (5) can be simplified as

$$\rho bh\frac{\partial^2 w}{\partial t^2}+EI\frac{\partial^4 w}{\partial x^4}=-\frac{\varepsilon_0 hc_f f_e(x)V_b}{g^2}V_{AC}. \quad (6)$$

The output current equation, Eq. (4), can be linearized by substituting in $w=0$ such that

$$i_0 = -\frac{\varepsilon_0 h c_f V_b}{g^2}\int_0^L f_e(x)\dot{w}\,dx. \tag{7}$$

The exact solution for the beam deflection is

$$w = \sum_{i=1}^{\infty} W_i(x)\eta_i, \tag{8}$$

where $W_i(x)$ is the mode shape of the ith mode and η_i is the modal coordinate for the ith mode. The relationship between V_{AC} and i_o can be defined for each mode of the resonator by applying the exact solution for a single mode to Eq. (6)[13] and inserting the result into Eq. (7). Therefore, Eq. (8) can be reduced to $w = W_i(x)\eta_i$. Applying the solution to Eq. (6), the equation of motion in modal coordinates is[13]

$$\ddot{\eta}_i + \frac{\omega_i}{Q_i}\dot{\eta}_i + \omega_i^2\eta_i = \frac{-\varepsilon_0 c_f V_b V_{AC}}{\rho b\gamma g^2}\int_0^L f_e(x)W_i(x)dx, \tag{9}$$

where $\gamma = \int_0^L W_i^2(x)dx$ and is used to normalize the mode shape. The resonance frequency of the ith mode, ω_i, is defined as

$$\omega_i = \pi^2\bar{\beta}_i^2\sqrt{\frac{E}{12\rho}}\frac{b}{L^2}, \tag{10}$$

with coefficients $\bar{\beta}_i = 1.506$, 2.5, 3.5, 4.5, 5.5… for $i = 1$, 2, 3, 4, 5,… A viscous damping term has been introduced in Eq. (9) to model energy dissipation in the beam, where Q_i is the quality factor of the ith mode. The mode shapes are

$$W_i(x) = \sinh\beta_i x - \sin\beta_i x + \alpha_i\cosh\beta_i x - \alpha_i\cos\beta_i x, \tag{11}$$

where

$$\alpha_i = \frac{\sinh\beta_i L - \sin\beta_i L}{\cos\beta_i L - \cosh\beta_i L}, \tag{12}$$

and $\beta_1 L = 4.73$, $\beta_3 L = 11.00$, and $\beta_5 L = 17.28$.

Applying the modal solution to Eq. (7) yields

$$i_0 = -\frac{\varepsilon_0 h c_f V_b}{g^2}\int_0^L f_e(x)W_i(x)dx\,\dot{\eta}_i. \tag{13}$$

Since the vibration modes are known to be well separated, the dynamic response of the resonator to an excitation frequency at a single resonance frequency can be accurately described by the equation of motion for only that mode. Therefore, the relationship between V_{AC} and i_o can be found by taking the Laplace transform of Eqs. (9) and (13) and combining the results such that

$$\frac{i_o(s)}{V_{AC}(s)} = \frac{\varepsilon_0^2 h L c_f^2 V_b^2 H_i}{\rho b g^4}\frac{s}{s^2 + \frac{\omega_i}{Q_i}s + \omega_i^2}, \tag{14}$$

where

$$H_i = \frac{1}{L\gamma}\left\{\int_0^L f_e(x)W_i(x)dx\right\}^2, \tag{15}$$

and s is the Laplace operator. Equation (14) yields the motional impedance for all of the resonator's modes, as described in Section III.

III. MOTIONAL IMPEDANCE ANALYSIS

The motional impedance for the ith mode, Z_{mi}, where $Z_{mi} = V_{AC}/i_{oi}$, is found by transforming Eq. (14) into the frequency domain such that

$$Z_{mi}(j\omega) = \frac{\rho b g^4\left(\omega_i^2 - \omega^2 + j\frac{\omega_i}{Q_i}\omega\right)}{j\varepsilon_0^2 h L c_f^2 V_b^2 H_i\omega}. \tag{16}$$

Equation (16) provides the impedance for a single mode as a function of frequency. In most cases, the impedance on resonance, or motional resistance, R_{mi}, is the real metric of interest. Evaluating Eq. (16) at resonance and taking the magnitude results in

$$R_{mi} = \frac{\rho b g^4\omega_i}{\varepsilon_0^2 h L c_f^2 V_b^2 Q_i H_i}. \tag{17}$$

This expression for motional resistance is similar to that shown in Refs. 14–16 but has the added benefit of including all mode numbers and possible electrode lengths. All of the terms in Eq. (17) are known material or geometric parameters with the exception of H_i and Q_i. As shown by Eq. (15), H_i, or the *H parameter*, is a function of the mode shape for the ith mode and the electrode length. Equation (15) can be solved analytically and evaluated over the full range of the electrode length. Values of H_i for the first three odd modes as a function of electrode length are shown in Fig. 2. Even modes are not presented because they are not transduced effectively with a symmetric electrode. Since Eq. (15) is nondimensional, the values in Fig. 2 apply to resonators of any size, making it easy to calculate the motional impedance assuming Q_i is known.

The results in Fig. 2 show that the peaks in H_i are located at the nodes for the respective mode and that the maximum value of H_i occurs when the electrode length is equal to the beam length for all modes. When comparing the maxima for the presented modes, H_1 is approximately 5.22 and 12.88 times greater than H_3 and H_5, respectively. Looking at the values for the third and fifth modes, an electrode greater than 87% and 92% of the beam length, respectively, will provide the best transduction of these modes. In practice, it is impossible to have an electrode with the same length as the beam due to proximity with the beam anchors, as shown in Fig. 1. Therefore, the optimal value is somewhere between 100% and the above stated values. Minimizing the motional resistance becomes increasingly difficult as the mode number increases because the peak value goes down and the width of the maximum peak near $L_e = 100\%$ gets smaller. Having derived Eq. (17), Section IV will focus on comparing the motional resistance and quality factor for different mode numbers operating at the same natural frequency.

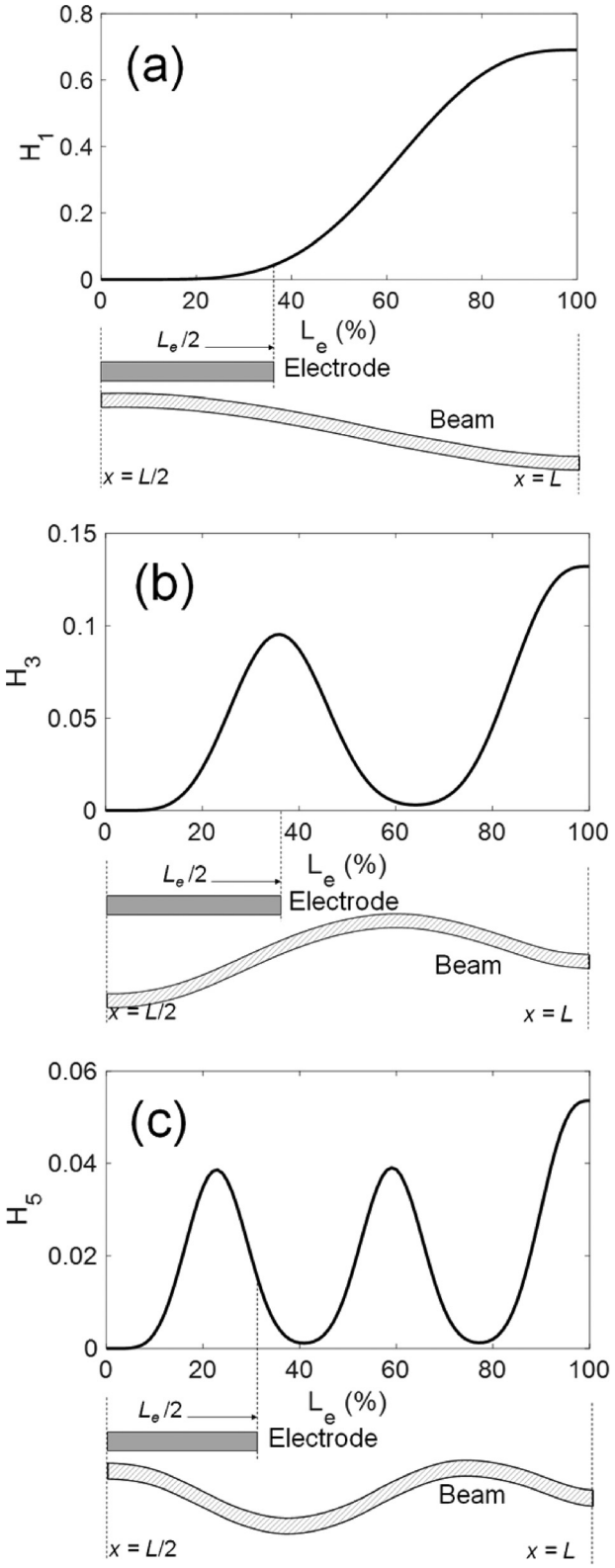

FIG. 2. H_i as a function of electrode length for modes (a) one, (b) three, and (c) five. Respective mode shapes (half of the beam) relative to the electrode length are included to show their influence on the parameter.

IV. MODE SELECTION

The electrostatic beam resonator can operate at its fundamental resonance frequency or in a higher mode of vibration. Therefore, two different resonators can be designed to have the same resonance frequency while operating in different modes. In this section, we start by looking at how the motional resistance derived in Section III can be used to determine the best mode number to select for a desired operating frequency. In order to compare the relative performance of two resonators, devices A and B, the ratio of the motional resistances of the two resonators will be examined. In this analysis, device A operates in its fundamental mode and device B operates in an odd higher mode. The motional resistance ratio between devices B and A, $R_{B/A}$, can be found using Eq. (17) and is written as

$$R_{B/A} = \left(\frac{g_B}{g_A}\right)^4 \left(\frac{V_{bA}}{V_{bB}}\right)^2 \frac{b_B}{b_A} \frac{h_A L_A H_A Q_A}{h_B L_B H_B Q_B}. \tag{18}$$

The subscripts, A or B, indicate the device for each parameter.

There are three important assumptions related to practical constraints on the resonator design and fabrication that will simplify the analysis of $R_{B/A}$. First, it is assumed that there is a maximum aspect ratio of beam width to thickness such that $b \leq h/\delta$, where δ is set by the etch process for the device layer, and devices A and B have the same δ. For example, δ is between 25 and 40 for deep reactive ion etching depending on the tool and process. Second, it is assumed that $g_A = g_B$. It is possible to fabricate small gaps without constraints on the beam thickness by using a trench refill approach[6] or a mechanism for reducing the gap during operation.[17] Therefore, we assume that these advanced approaches would be used when pushing the performance limits. Finally, the bias voltage, V_b, is assumed to be the same for devices A and B. The break down voltage of a vacuum gap, which is typically around 300 V for silicon,[18] is much higher than the bias voltage range used in most applications. Furthermore, the electrostatic force due to V_b is balanced such that pull-in can only occur due to a combination of a large V_{AC} and V_b.

Noting these assumptions, from Eq. (18), the ratio of the motional resistance ratio can be reduced to

$$R_{B/A} = X_{A/B} Q_{A/B}, \tag{19}$$

where $X_{A/B} = L_A H_A / L_B H_B$ and $Q_{A/B} = Q_A / Q_B$. In order to determine which resonator has the lower motional resistance, quality factors must be known, either through experiments or modeling. Before including quality factor values in this analysis, it is useful to look at the parameter $X_{A/B}$. In order to provide fair and reasonable comparisons between modes, three specific scaling conditions relating Devices A and B are described here and used in the following analysis.

Case 1 assumes the same beam width for devices A and B, $b_A = b_B$. Using this relationship, the following can be obtained from Eq. (10):

$$X_{A/B} = \frac{\bar{\beta}_A}{\bar{\beta}_B} \frac{H_A}{H_B}. \tag{20}$$

Case 2 constrains the resonators to have the same bending stiffness such that

$$X_{A/B} = \left(\frac{\bar{\beta}_A}{\bar{\beta}_B}\right)^{8/5} \frac{H_A}{H_B}. \quad (21)$$

This is derived from the static stiffness of a doubly clamped beam defined at the center of the beam and the requirement that devices A and B have the same resonance frequency.

Finally, case 3 requires devices A and B to have the same aspect ratio of length to width. A fixed aspect ratio will significantly reduce the difference in compliance between the fundamental mode and higher mode resonators, making it a reasonable design choice. Applying a fixed aspect ratio to Eq. (10), where the natural frequency for devices A and B is the same, results in

$$X_{A/B} = \left(\frac{\bar{\beta}_A}{\bar{\beta}_B}\right)^{2} \frac{H_A}{H_B}. \quad (22)$$

Note that Eqs. (20)–(22) are the same except for the exponent on $\bar{\beta}_A/\bar{\beta}_B$, where the exponent is defined by the scaling law and ranges from 1 to 2 for the three cases. These three cases span a wide range of the design space when scaling between resonators

The analysis of Eqs. (20)–(22) shows that $X_{A/B}$ is smallest when $L_e = L$ as long as $L_e > 0.34\ L$ for $X_{1/3}$ and $L_e > 0.26\ L$ for $X_{1/5}$. Since there is no practical reason to choose an electrode length shorter than $0.34\ L$, comparing the resonators with $L_e = L$ will provide the best case scenario for higher mode resonators. For $L_e = L$, it was found that $X_{1/3} = 2.25$ and $X_{1/5} = 3.53$ for case 1, $X_{1/3} = 1.35$ and $X_{1/5} = 1.62$ for case 2, and $X_{1/3} = 0.97$ and $X_{1/5} = 0.97$ for case 3. Therefore, in general, if $Q_{A/B} \geq 1$, then $R_{B/A} \geq 1$. This means that if it can be determined that $Q_{A/B} \geq 1$, then the fundamental mode resonator would be the optimal choice in terms of motional resistance and quality factor. Only the first three odd modes are considered in this analysis for brevity but higher modes could be investigated without any changes in approach.

The optimal mode number is the one with the lowest motional resistance, R_{mi}, and highest quality factor, Q_i, although it may not always be that simple, as discussed below. Equation (19) and the quality factor ratio, $Q_{A/B}$, can be used to determine the optimal mode number. Clearly, if $R_{B/A} < 1$ and $Q_{A/B} < 1$, then the device B is the better resonator and vice versa. In order to push the analysis further, models for quality factor that have previously been experimentally validated are now introduced. The two dominant sources of energy dissipation for vacuum packaged electrostatic beam resonators are thermoelastic dissipation[19,20] and anchor loss.[21] Surface dissipation can also play a role in the quality factor, particularly for nanoscale resonators.[22,23] However, it has been shown that surface dissipation can largely be mitigated in microscale resonators through surface treatment.[21] Another possible source of energy dissipation is pressure damping due to molecular interactions with the resonator. However, it has been shown that for vacuum packaged beam resonators operating at or below 1 Pa, which is now easily attainable in hermetic packaging, pressure damping is negligible.[24] As a result, surface dissipation and pressure damping are ignored in this analysis.

The quality factor due to thermoelastic dissipation[25] can be modeled as

$$Q_{TED} = \left(\frac{c_p \rho}{E \alpha^2 T_0}\right) \frac{1 + (\omega\tau)^2}{\omega\tau}, \quad (23)$$

where

$$\tau = \left(\frac{b}{\pi}\right)^2 \frac{c_p \rho}{\kappa}, \quad (24)$$

and c_p is the specific heat, κ is the thermal conductivity, α is the coefficient of thermal expansion, and T_0 is the equilibrium temperature of the beam. Q_{TED} can be calculated at any angular frequency, ω, and the above model is used for all modes, although with limitations in accuracy for the higher modes. This model has been shown to be reasonably accurate in predicting the quality factor when $\omega \approx \tau$,[25–27] which is when thermoelastic dissipation is typically much larger than anchor loss. Outside of this range, the combination of thermoelastic dissipation and anchor loss must be considered.

The quality factor due to anchor loss[21] for a clamped-clamped beam can be modeled as

$$Q_a = \varphi \left(\frac{2.43}{(3-\upsilon)(1+\upsilon)} + \frac{1.91}{\prod}\right) \frac{1}{(\bar{\beta}_i \chi_i)^2} \left(\frac{L}{b}\right)^3, \quad (25)$$

where υ is the Poisson's ratio and $\prod$ and χ_i are defined in Ref. 21. A correction factor, φ, where $\varphi = 0.263$, was added to the original equation[21] because it was found that there is a consistent multiplicative error of 0.263 between the calculations and the values reported in Ref. 21 for a doubly clamped beam. The effective quality factor is then defined as $Q_{tot} = Q_{TED} Q_a / (Q_{TED} + Q_a)$. Note that Q_{tot} is a function of the beam length and width, but not the beam thickness and gap size. Equations (23)–(25) have been shown experimentally to be reasonably accurate for beam resonators operating at 1 MHz and below.[21,28] For example, the error range and mean error for this model have been shown to be +2.9% to +80% and 32.2% for atomic force microscopy (AFM) cantilevers[28] and −17.2% to 6.5% and 7.0% for electrostatic beam resonators,[21] respectively. A positive error indicates an overestimate of the quality factor. While the error range is large, particularly for the AFM cantilevers, the model still provides sufficient fidelity for this comparison, as will be discussed in detail later.

Quality factor has been calculated using the above model for silicon resonators since silicon is the most commonly used material for these devices. The material properties for silicon used in the analysis are $\rho = 2329\ \text{kg/m}^3$, $E = 130\ \text{GPa}$, $\upsilon = 0.28$, $\alpha = 2.6 \times 10^{-6}\ \text{1/K}$, $c_p = 712\ \text{J/(g K)}$, $\kappa = 90\ \text{W/(m K)}$, and $T = 300\ \text{K}$.[29,30] The beam width and resonance frequency ranges considered here are $1\ \mu\text{m} \leq b \leq 20\ \mu\text{m}$ and $100\ \text{kHz} \leq f_n \leq 20\ \text{MHz}$, respectively, which covers most of the beam resonators found in the literature. Using the calculated quality factors, $Q_{A/B}$ was evaluated for all three scaling cases described above and for comparisons between the fundamental mode and the third and fifth modes.

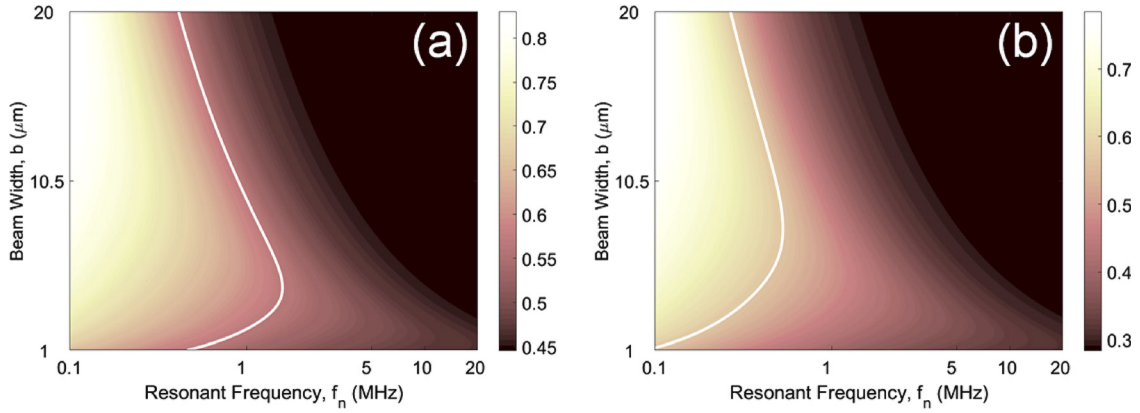

FIG. 3. $Q_{A/B}$ for case 1 (same beam width). (a) Device B operated in the third mode and (b) device B operated in the fifth mode. White contour line represents $Q_{A/B} = 0.57$.

The results for case 1 are shown in Fig. 3, where the beam width shown on the y axis is for device A (fundamental mode). Figure 3 shows that $Q_{A/B}$ is less than one throughout the entire parameter range, meaning that device B always has a higher Q for this case. Specifically, $0.45 < Q_{1/3} < 0.84$ and $0.28 < Q_{1/5} < 0.80$. Assuming $L_e = L$ and substituting the $Q_{A/B}$ bounds into Eq. (19) results in $1.0 < R_{3/1} < 1.89$ and $0.99 < R_{5/1} < 2.82$. Therefore, the motional resistance of device A is generally smaller than or equal to device B. Clearly, there is a tradeoff between R_m and Q for case 1, such that mode selection in this case is based on which parameter is more important for the application.

Figure 4 shows the $Q_{A/B}$ results for case 2. When the resonators have the same stiffness, the quality factor is always better for the fundamental mode resonator, where the ranges for $Q_{A/B}$ are $1.13 < Q_{1/3} < 5.18$ and $1.19 < Q_{1/5} < 12.86$. The corresponding ranges for $R_{B/A}$ are $1.53 < R_{3/1} < 7.0$ and $1.93 < R_{5/1} < 20.83$. Therefore, these results indicate that the fundamental mode is always the optimal mode for case 2.

Finally, $Q_{A/B}$ was calculated for case 3, as shown in Fig. 5. The quality factor for the fundamental mode resonator is larger than for the higher modes throughout the entire parameter space, where $1.92 < Q_{1/3} < 17.21$ and $4.0 < Q_{1/5} < 78.06$. Similarly, the motional resistance of device A is significantly lower than device B over the entire parameter range where $1.86 < R_{3/1} < 16.69$ and $3.88 < R_{5/1} < 75.72$. This analysis indicates that when the aspect ratio of length to width is equal for all resonators, the fundamental mode resonator will outperform higher mode resonators in both quality factor and motional resistance by at least nearly a factor of two and significantly more in most cases.

The results for the three cases point to higher modes always having a larger motional resistance. Furthermore, the fundamental mode resonator will have higher quality factor for cases 2 and 3 and the higher mode resonator will achieve higher Q for case 1. For case 1, device B must be longer than device A by a factor of $\bar{\beta}_B/\bar{\beta}_A$ (2.32, 3rd mode; 3.65, 5th mode) in order to have the same resonance frequency. The higher mode resonators are therefore significantly more compliant (12.49X, 3rd mode; 48.63X, 5th mode) making them more likely to fail in fabrication and in the field, thereby limiting their feasibility. Recall that it was assumed that $L_e = L$ and $g_a = g_b$. In practice, $L_e < L$ and in many cases $g_a < g_b$, pushing these conclusions further in favor of the fundamental mode.

The above conclusions are based on the assumption that the quality factor model is perfect, which of course is not true. It is therefore useful to look at how tolerant the above conclusions are to model uncertainty. If the uncertainty is large enough, $Q_{A/B}$ could be greater than one for case 1 or less than one for cases 2 and 3, thereby changing the conclusions in the above analysis. In order to analyze how much

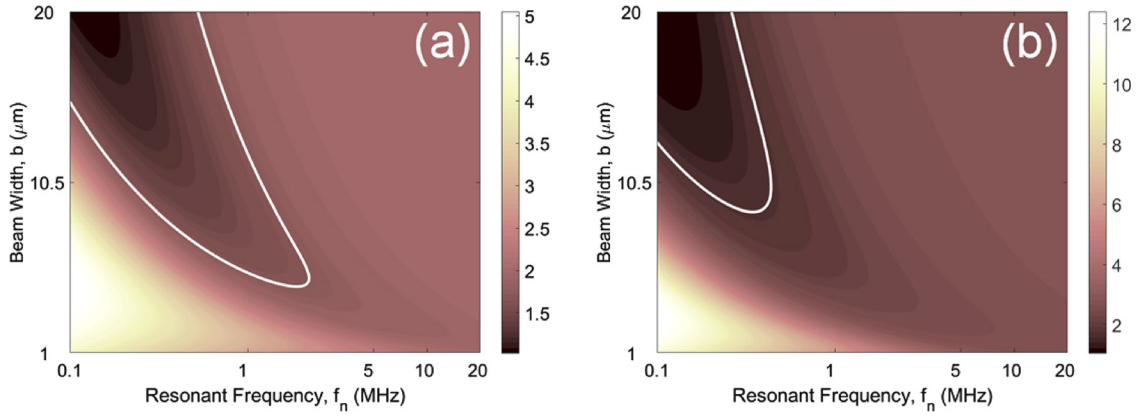

FIG. 4. $Q_{A/B}$ for case 2 (same bending stiffness). (a) Device B operated in the third mode and (b) device B operated in the fifth mode. White contour line represents $Q_{A/B} = 1.75$.

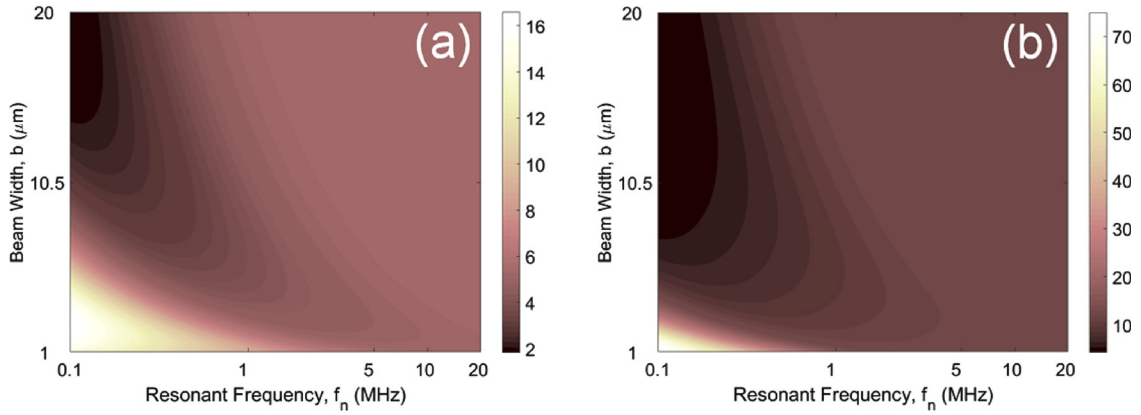

FIG. 5. $Q_{A/B}$ for case 3 (same aspect ratio). (a) Device B operated in the third mode and (b) device B operated in the fifth mode.

the values of $Q_{A/B}$ shown in Figs. 3–5 can change due to model uncertainty, the maximum modeling errors demonstrated in previous results are used. As stated earlier, the model error was found experimentally to be in the range of $+2.9\%$ to $+80\%$ for AFM cantilevers[28] and -17.2% to $+6.5\%$ for electrostatic beam resonators.[21] The results from the first example are used here since they yielded a larger error distribution. For case 1, if Q_A is off by $+2.9\%$ and Q_B is off by $+80\%$, which is the worst case for this error range, $Q_{A/B}$ must be less than 0.57 for the conclusions for case 1 to hold. Similarly, $Q_{A/B}$ must be greater than 1.75 for cases 2 and 3. These values are equivalent to being tolerant to $\pm 27.3\%$ modeling error in all three cases if the uncertainty in Q_A and Q_B is assumed to be the same but with opposite sign.

Looking at Fig. 3, where the white contour line represents $Q_{A/B} = 0.53$, it is clear that $Q_{A/B} < 0.53$ for the majority of the parameter space for case 1. Similarly, $Q_{A/B} > 1.75$ throughout most of the parameter space for case 2, as shown in Fig. 4. Finally, $Q_{A/B} > 1.75$ for case 3 without exception (see Fig. 5). While not definitive, these results provide reasonable confidence that the fundamental mode resonator will have the higher quality factor for cases 2 and 3, while the higher mode resonator will have the greater quality factor for case 1, with some exceptions that are shown in Figs. 3 and 4.

There are two caveats to these conclusions on mode selection that warrant further consideration. First, surface dissipation was ignored in this analysis because it has been shown that it can be mitigated through surface treatment.[21] However, it may play a major role in the quality factor for deeply scaled resonators. Second, to our knowledge, the anchor loss model, Eq. (25), has only been validated experimentally up to 1 MHz, such that the upper part of the presented frequency range remains unvalidated. These issues require further experimental investigation to provide a more definitive conclusion on selecting the mode number with the best motional resistance and quality factor. If other energy dissipation models are found to more accurately predict the quality factor, the equations derived here will still provide a concise approach for selecting the mode number for optimal performance.

V. CONCLUSION

A dynamic model for electrostatic beam resonators has been derived that describes the relationship between the input voltage, V_{AC}, and output current, i_o, for all modes and for varying electrode length. This model has been used to derive the motional resistance for each mode as a function of electrode length. The resulting equations were used to establish two performance metrics for comparing two resonators operating at the same frequency but in different modes: the motional resistance ratio and quality factor ratio. Using an accepted model for quality factor that has previously been experimentally validated, the quality factor can be calculated. This can then be used to find the motional resistance ratio and quality factor ratio between the two resonators. It was found that if the quality factor of a fundamental mode resonator is greater than that of a higher mode resonator operating at the same resonance frequency, then the fundamental mode resonator would also have lower motional resistance, making it the better choice.

This approach for mode selection was demonstrated for three geometric scaling cases between the fundamental and higher mode resonators: case 1: same beam width; case 2: same bending stiffness; and case 3: same aspect ratio (length/width). The results indicate that the fundamental mode provides a lower motional resistance for all three cases. Furthermore, the quality factor is higher in the fundamental mode resonator except in case 1, where the width of the two resonators is the same. The resulting long slender beam resonators operating in a higher mode for case 1 are generally not desirable since they are more likely to fail during fabrication and operation due to their significantly lower stiffness. As a result, the outcome of the presented analysis is that the fundamental mode will generally provide the best performance for silicon resonators. This assertion could change for different materials and geometric constraints. An analysis of the effect of uncertainty in the quality factor model found that the mode selection conclusions would hold throughout most of the parameter space for beam geometry if the bounds on modeling error are the same as found in previous work. The derived equations and method for optimal mode selection provide a clear framework for comparing resonators and are compatible with any quality factor model, which we expect will improve in accuracy in the future.

[1]C.T.-C. Nguyen, Proc. SPIE **5715**, 11–25 (2005).
[2]C. T.-C. Nguyen, IEEE Trans. Ultrason., Ferroelectr., Freq. Control **54**, 251–270 (2007).

[3]J. T. M. Van Beek and R. Puers, J. Micromech. Microeng. **22**, 013001 (2012).
[4]W. Pang *et al.*, Lab Chip **12**, 29–44 (2012).
[5]H. C. Nathanson *et al.*, IEEE Trans. Electron Devices **14**, 117–133 (1967).
[6]S. Pourkamali *et al.*, J. Microelectromech. Syst. **12**, 487–496 (2003).
[7]M. Agarwal *et al.*, Appl. Phys. Lett. **89**, 214105 (2006).
[8]R. M. C. Mestrom *et al.*, Sens. Actuators, A **162**, 225–234 (2010).
[9]N. Kacem *et al.*, Nanotechnology **20**, 275501 (2009).
[10]S. T. Bartsch *et al.*, ACS Nano **6**, 256–264 (2012).
[11]M. U. Demirci and C. T.-C. Nguyen, in *Proceedings of the IEEE Frequency Control Symposium* (2003), pp. 810–818.
[12]M. Younis *et al.*, J. Microelectromech. Syst. **12**, 672–680 (2003).
[13]L. Meirovitch, *Fundamentals of Vibrations* (McGraw-Hill, New York, 2001), p. 549.
[14]G. K. Ho *et al.*, in *Proceedings of the IEEE MEMS*, 2005, pp. 116–120.
[15]M. Agarwal *et al.*, J. Appl. Phys. **102**, 074903 (2007).
[16]H. K. Lee *et al.*, in Proceedings of the IEEE Frequency Control Symposium (2011), pp. 1–6.
[17]E. J. Ng *et al.*, in Proceedings of the IEEE MEMS (2015), pp. 1281–1284.
[18]C.-H. Chen, J. A. Yeh, and P.-J. Wang, J. Micromech. Microeng. **16**, 1366–1373 (2006).
[19]C. Zener, Phys. Rev. **53**, 90 (1937).
[20]R. Lifshitz and M. L. Roukes, Phys. Rev. B **61**, 5600 (2000).
[21]Z. Hao, A. Erbil, and F. Ayazi, Sens. Actuators, A **109**, 156–164 (2003).
[22]J. Yang, T. Ono, and M. Esashi, J. Vac. Sci. Technol., B **19**, 551 (2001).
[23]M. Imboden and P. Mohanty, Phys. Rep. **534**, 89–146 (2014).
[24]S. Ghaffari *et al.*, J. Microelectromech. Syst. **24**, 276–288 (2015).
[25]R. Candler *et al.*, J. Microelectromech. Syst. **15**, 927–934 (2006).
[26]T. V. Roszhart, *Proceedings of the Solid-State Sensor and Actuator Workshop* (1990), pp. 13–16.
[27]R. N. Candler *et al.*, in *Proceedings of the Solid-State Sensor and Actuator Workshop* (2003), pp. 332–335.
[28]J. Lübbe *et al.*, Meas. Sci. Technol. **21**, 125501 (2010).
[29]M. A. Hopcroft, W. D. Nix, and T. W. Kenny, J. Microelectromech. Syst. **19**, 229 (2010).
[30]J. F. Shackelford and W. Alexander, *CRC Materials Science and Engineering Handbook*, 3rd ed. (CRC Press, Boca Raton, FL, 2000).